ORIGINAL PAPER

Modeling Uniform Flow of Couple Stress Non-Newtonian Fluids in Porous Media Using a Cell-Based Framework

Shyamala Sakthivel*

Excel Engineering College (Autonomous), Namakkal, Tamilnadu, India

Correspondence
*Shyamala Sakthivel, Excel Engineering College (Autonomous), Namakkal, Tamilnadu, India

Summary

This study explores the application of the cell model to uniform flow through a couple stress fluid enveloped by a porous medium. The governing equations include the Brinkman equation for flow within the porous spherical shell and the Stokes equation for the couple stress fluid droplet. The velocity components are derived using stream functions, with boundary conditions incorporating mutual impenetrability, continuity of tangential velocity and stresses, vanishing couple stresses, and constraints defined by Happel, Kuwabara, Kvashnin, and Mehta-Morse (Cunningham's framework). Analytical solutions for the axisymmetric flow field are obtained via the method of separation of variables, enabling explicit expressions for the pressure distribution and stream function. The study quantifies the drag force and drag coefficient, investigating the influence of parameters such as permeability, viscosity ratios, the couple stress viscosity ratio, and the couple stress parameter. Graphical analyses illustrate the relationship between these parameters and the hydrodynamic drag and permeability. The results are applicable to various scenarios involving fluid flow around porous spherical bodies, including natural and engineered materials such as permeable rocks, aloxite, sand beds, soils, and petroleum reservoir formations. Additionally, the findings provide valuable insights for optimizing the design of advanced bearing systems and other engineering applications.

KEYWORDS:
Brinkman equation, unit cell model, couple stress fluid, stream function, Gegenbauer function, hydrodynamic drag force, hydrodynamic permeability, non-dimensional drag coefficient.

1 | INTRODUCTION

Joseph and Tao[1] explored the impact of permeability on the slow motion of a porous spherical object immersed in a viscous fluid. This topic has garnered significant interest due to its applications in geophysics, industry, and engineering, leading to numerous studies focused on analyzing the flow of viscous fluids through and around porous bodies using both analytical and numerical approaches. The foundational theory of couple stress fluids, which accounts for additional stress and couple stress vectors acting on fluid surfaces, was introduced by Stokes[2]. He provided solutions to the creeping flow problem for couple stress fluids around a spherical particle. These fluids are characterized by asymmetric stress tensors, body couples, and couple

[0] **Nomenclature:** a_o, radius of solid spherical core; a, radius of solid spherical droplet; b, radius of solid porous container; U, uniform velocity; E^2, Stokesian operator; β, couple stress parameter; $\psi^{(i)}(r, \theta)$, stream functions; $F^{\sim}$, Hydrodynamic drag force; L_{11}, Hydrodynamic permeability; $G_2(\theta)$, Gegenbauer function of first kind; R, Θ, ϕ, spherical polar co-ordinates; δ_{ij}, Kronecker delta

stress tensors, all of which are influenced by the curvature twist rate tensor[3,4]. The behavior of couple stress fluids is governed by constitutive equations analogous to the classical Navier–Stokes equations but incorporating tensors for stresses and couple stresses. Analytical investigations, such as those by Rao and Iyengar[5] on flow past axisymmetric bodies, and by Ramkisson[6], who developed a practical formula for drag on axisymmetric bodies, have enriched the field. Additionally, studies on couple stress fluid dynamics under no-slip conditions have been conducted by Devakar and Iyengar[7]. Other research, such as Padmavathi and Amaranth[8] on viscous fluid flow through permeable spheres, and Zlatanovski[10] on axisymmetric Stokes flow around porous prolate spheroids, highlights the depth of exploration in this domain. Qin and Kaloni[9] also addressed the creeping flow around porous spherical shells, while Ramana Murthy et al. [11] examined these flows in the context of couple stress fluids. The Navier-Stokes framework for couple stress fluids plays a pivotal role in understanding various practical problems, especially in biomedical applications such as modeling blood flow, synovial joint mechanics, and certain oils. By leveraging these mathematical models, researchers can predict fluid behavior with high fidelity. These fluids, which exhibit asymmetric stress tensor behavior and length-dependent effects, allow for the inclusion of couple stresses and body couples, offering a richer understanding of fluid mechanics in complex systems.

Happel[12,13] proposed a model where shear stress on the surface of a cell diminishes, indicating the absence of friction caused by particle interactions within a swarm. Kuwabara[14] introduced the assumption of zero vorticity on the cell boundary, implying that the velocity curl vanishes at the surface. Kvashnin[15] considered a symmetry condition for velocity, positing that the radial component of velocity approaches extreme values on the cell surface. Cunningham, along with Mehta and Morse[16], assumed that the tangential velocity is proportional to the mean fluid velocity, reflecting continuity in flow dynamics at the unit cell boundary. Saad[17,18] advanced this line of research by investigating Stokes flow around clusters of axially symmetric porous spheroids and irregular spherical fragments using the unit cell modeling approach. Additionally, Saad systematically studied the quasi-steady axially symmetric flow of an incompressible viscous fluid through a collection of porous convex spheres within cell models, incorporating all four major boundary conditions typically applied at the cell boundary. This comprehensive analysis extended to micropolar fluids, further enriching the understanding of fluid behavior in complex cell configurations. Aparna et al. [19,20] studied the oscillatory motion of a couple stress fluid flowing through a permeable medium. They found that the drag force experienced by a viscous fluid was lower compared to that of a couple stress fluid, indicating that couple stress fluids offer greater resistance to flow. In a separate investigation, the authors explored the flow induced by the rotation and oscillation of a permeable sphere in an unbounded region of incompressible fluid. Their findings revealed that, due to the presence of couple stresses, the velocity of the fluid particles near the surface of the sphere exceeded that of the sphere's surface itself.

Devakar and Shankar[21,22] provided closed-form analytical solutions for uniform directional flows of couple stress fluids, specifically analyzing Poiseuille flow, Couette flow, and Couette-Poiseuille flow between two concentric circular cylinders with a porous layer under slip boundary conditions. Subsequently, they investigated the influence of magnetohydrodynamics (MHD) on the peristaltic propulsion of couple stress fluid in a tube containing an endoscope. Their study revealed that the application of a uniform magnetic field resists the flow, while the pumping rate in the peristaltic flow increased when transitioning from a horizontal to a vertical channel. Shehadeh and Ashmawy[23] examined the rotating oscillations of a rigid domain within an incompressible couple stress fluid. They found that the motion was induced by the sudden oscillation of the rigid sphere, which rotated about an axis passing through its core, with a time-dependent angular velocity. Alsudais et al. [24] conducted an analytical investigation into the semi-standard translational motion of an incompressible couple stress fluid constrained between two eccentric spherical geometries. Radhika et al. [25] explored the creeping or Stokes flow of a viscous fluid around a system of two porous spheres, employing a bipolar coordinate system for the problem's formulation. Building on this, Radhika and Rani[26] analytically addressed the viscous flow dynamics beyond a pair of divided porous spheres, highlighting that the internal pressure distribution is influenced by dimensionless parameters related to the medium's permeability and the fluid's viscosity. Srinivasacharya and Sreenath[27] examined the unsteady bioconvective flow of a couple stress fluid containing motile microorganisms between parallel plates. They utilized the successive linearization technique to linearize the governing nonlinear equations, which were then solved numerically using the Chebyshev collocation method. Surabhi et al. [28] investigated the interplay of geometric parameters with hemodynamic and rheological properties, focusing on the Newtonian nanofluid flow in a bifurcated arterial structure with atherosclerotic deposits in the presence of a catheter.

The couple stress Nano-fluid has a higher wall shear stress compared to Newtonian Nano-fluid. Filippov et al. [29] using the cell model to conduct a numerical study of a Stokes-Brinkman method with differing fluid viscosity that represents fluid flow along this pair of partially porous parallel cylindrical particles to form a fibrous membrane. Flow throughout a Reiner–Rivlin liquid sphere, which is enclosed by a Newtonian liquid exterior and placed into a penetrable medium, is explored by Selvi et al.[30,31]. Utilizing the unit cell model technique, Khanukaeva et al.[32] investigated the flow of micropolar fluid through

a membrane modelled as a swarm of solid cylindrical particles with a permeable layer and they calculated the drag force on a non-Newtonian fluid sphere embedded in a permeable region placed in a another non-Newtonian fluid. Shukla and Ramalakshmi[33] explored the uniformly steady flow of axially symmetric, incompressible couple stress fluid passing through a solid-cored fluid sphere. The component of velocity profile are calculated using stream functions, and the sphere's surface is subjected to a non-slip limit constrain and vanishing couple stress condition. Geetha Vani and Ravi Kanth[34] analyzed the issue of oscillatory flow of a non-compressible couple stress fluid yielded by the rotary oscillating of two concentric spherical body. Shyamala et al. [35,36,37,38] investigated the uniform motion of a couple stress fluid over a permeable sphere. Abdelsala et al. [39,40] visualizing the electroosmotic flow of immiscible fluids through a porous medium in vertical annular microtubes. This paper aims to study the behavior of a non-Newtonian nanofluid in an asymmetric channel due to peristaltic waves. The generation of thermal radiation and activation energy is also taken into account.[41] unravelling the behavior of a hybrid nanofluidic model made up of silica nanoparticles and nanodiamonds. Three different configurations of catheterized tapered arteries converging, non-tapered, and diverging are used by the nanofluid to spread through them.

According to this literature survey and to the best of the author's knowledge, the impact of the hydrodynamic drag force and hydrodynamic permeability acting on a couple stress fluid sphere enclosed by a porous sphere in cell model technique has yet to be analyzed. The purpose of this study is to explore the cell model for uniform fluid flow through a couple stress fluid covered by a porous medium. The Brinkman and Stokes equations govern the flow through the porous spherical container and the couple stress fluid spherical droplet respectively. The components of the velocity profile are calculated by using stream functions, and the sphere's surface is subjected to kinematic viscosity of mutual impenetrability, the continuity of tangential velocity and tangential stresses, vanishing couple stresses, Happel, Kuwabara, Kvashnin, and Mehta-Morse (Cunningham's) boundary constraints. For the axially symmetric motion, both pressure distribution and the stream function solution are explicitly solved. The method of variable separation is used to investigate an analytical resoluteness for the flow field. The drag force on an Uniform fluid flow through a non-Newtonian couple stress fluid covered by a porous medium in cell model and the drag coefficient are calculated, and the impacts of the permeability, the ratio of viscosity, the couple stress viscosity ratio, and the parameter of couple stress . The appropriate dependencies are graphically delineated and reviewed, including the permeability, couple stress parameter, viscosity ratio, and couple stress viscosities. The consequences of a wide range of appropriate parameters on hydrodynamic drag force and hydrodynamic permeability have been examined and graphically presented. Thus, the discoveries of this article are comprehensively pertinent to the investigation of the flow of permeable liquids past spherical permeable rocks, aloxite materials, sand beds, earthen soil, petrol supply rocks, etc. The present application will support in planning a productive bearing framework.

2 | PROBLEM FORMULATION AND METHOD OF SOLUTION

Let us consider a solid spherical core with radius 'a_o' which is enclosed by a couple stress fluid spherical droplet with radius 'a' and viscosity 'μ_2' and couple stress parameter 'β' along the positive 's' direction. This fluid spherical droplet is enclosed by a hypothetical spherical porous container of radius 'b' shown in figure 1 . The inside medium we pass through must be homogeneous and isotropic. Further, we through to be the internal medium is additionally steady and incompressible. The flow is uniform axisymmetric with ignorance of body force and couples. The fluid spherical droplet must be stationary with its centre at origin of the spherical coordinate system (R, Θ, ϕ). The radius 'b' of a hypothetical cell is also chosen that the ratio of particle to cell volume is equal to the volume fraction ' '. The regions $a \le r \le b$ and $r \le a$ are indicated by region 1 and 2 respectively.

For the outside region of the fluid spherical droplet, the governing Brinkman equations for the porous medium can be found by Zlatanovski[10].

$$diu\ \mathbf{q}^{(1)} = 0, \tag{1}$$

$$\mathrm{A}^2\ \mathbf{q}^{(1)} - \left(\frac{a}{b}\right)^2 \mathbf{q}^{(1)} = \frac{1}{\mu_e}\,\mathrm{A}\,p^{(1)}, \tag{2}$$

where, $\mathbf{q}^{(1)}$- velocity of the fluid, $p^{(1)}$ - pressure, μ_e - effective viscosity.

In the case of creeping flow of incompressible couple stress fluids, the equations of motion are

$$t_{ji,j} + f_i = 0, \tag{3}$$

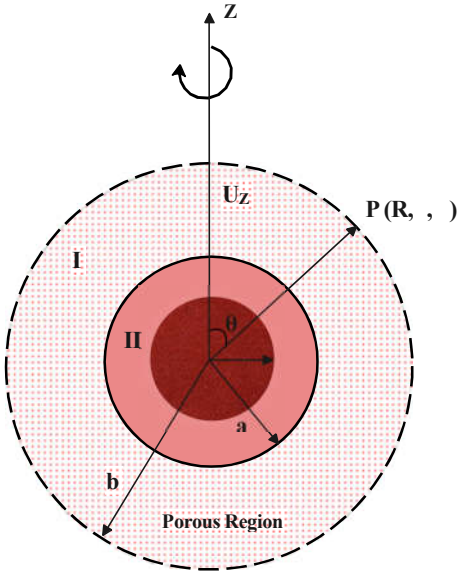

FIGURE 1 Physical representation of the problem

$$m_{ji,j} + s_{ijk}\, t_{jk} + I_i = 0. \tag{4}$$

The linear constitutive equations are provided by Stokes[2]

$$t_{(ij)} = -p\,\delta_{ij} + \mu\,(\mathbf{q}_{i,j} + \mathbf{q}_{j,i}), \tag{5}$$

$$m_{ij} = \frac{1}{3} m_{rr}\,\delta_{ij} + 4\eta\, k_{ij} + 4\eta^{f} k_{ji}. \tag{6}$$

Together with the continuity equation

$$\mathbf{q}_{i,i} = 0, \tag{7}$$

where t_{ij} - component of the stress tensor, m_{ij} - component of the couple stress, k_{ij} - component of the curvature twist rate tensor, p - pressure, $\mathbf{q}$ - velocity vector, f - body force, δ_{ij} - Kronecker delta, I - body couple, s_{ijk} - alternating tensor, (μ, η, η^{f}) are constants characteristics of the couple stress fluid and $t_{(ij)} = \frac{1}{2}\left(t_{ij} + t_{ji}\right)$.

The following field equations governing the motion of Stokes[2,3] couple stress fluid are deduced using the above equations,

$$\mathrm{A}.\ \mathbf{q}^{(2)} = 0, \tag{8}$$

$$\mu_2 \mathrm{A}^2\, \mathbf{q}^{(2)} - \eta \mathrm{A}^4\, \mathbf{q}^{(2)} - \mathrm{A}\, \mathbf{q}^{(2)} = -f - \frac{1}{2}\mathrm{A}x\, I. \tag{9}$$

In the ignorance of the body force and couples, the equations of motion for a Stokes couple stress fluid is followed by

$$\mathrm{A}.\ \mathbf{q}^{(2)} = 0, \tag{10}$$

$$\mathrm{A}\, p^{(2)} = \mu_2 \mathrm{A}^2\, \mathbf{q}^{(2)} - \eta \mathrm{A}^4\, \mathbf{q}^{(2)}. \tag{11}$$

Let us introduced the material quantities satisfying the ensuring inequalities by Stokes[2]

$$\mu \geq 0, \quad \eta \geq \eta^{f}, \quad \eta \geq 0. \tag{12}$$

We providing the solution in dimensionless form by bringing up the following non-dimensional variables

$$R = ar^{\sim},\ \psi^{(i)} = U a^2 \tilde{\psi}^{(i)},\ p^{(i)} = \frac{\mu_i U}{a} p^{\sim(i)},\ u_{\phi}^{(i)} = \frac{U}{a} u^{\sim(i)},\ r_{ij} = \frac{\mu_i U}{a} r^{\sim}_{ij}. \tag{13}$$

Where U and $^{f}a^{f}$ represent velocity of the flow and length of the flow field respectively.All flow functions are independent of $ø$ because the flow field is the meridian plane and the flow is axially symmetric. Happel and Brenner introduced the stream function ψ which satisfies the continuity equations and is associated with the velocity in the spherical coordinates system (R, Θ, $ø$).

$$\mathbf{q}^{(i)} = \mathbf{q_r}^{(i)}(r, \Theta)\, e\hat{}_r + \mathbf{q_\theta}^{(i)}(r, \Theta)\, e\hat{}_\Theta, \quad i = 1, 2. \tag{14}$$

Where, $e\hat{}_r$, $e\hat{}_\Theta$ are unit vectors. The velocity profiles of both regions are described as far as stream function as follows,

$$\mathbf{q}_{\mathbf{r}}^{(i)} = -\frac{1}{r^2 \sin\Theta}\frac{6\psi^{(i)}}{6\Theta}, \qquad \mathbf{q}_{\boldsymbol{\theta}}^{(i)} = \frac{1}{r\sin\theta}\frac{6\psi^{(i)}}{6r}. \tag{15}$$

Further abolishing the pressure from equation (2) and (11) using in equation (14), we get

$$E^2 \quad E^2 - a^2 \quad \psi^{(1)} = 0, \tag{16}$$

$$E^4 \quad E^2 - \beta^2 \quad \psi^{(2)} = 0. \tag{17}$$

Where, $E^2 = \frac{6}{6r^2} + \frac{\sin\Theta}{r^2}\frac{6}{6\theta} \quad \frac{1}{\sin\Theta}\frac{6}{6\theta}$, and permeability parameter $a^2 = \frac{b^2}{z}$ and $\beta^2 = \frac{\mu}{\eta}$.

The solution of the Brinkman equation (16) can be written as,

$$\psi^{(1)}(r, ()) = \overset{4}{A}_1 r^2 + \frac{B_1}{r} + C\, y_{1\ -2}(ar) + D\, y_{1\ 2}(ar) \overset{5}{G}_2(()). \tag{18}$$

The regular solution of the inner region is given by,

$$\psi^{(2)}(r, ()) = \frac{\overset{4}{A}_2}{r} + B\, \underline{r} + C_2 \ 1 + \frac{1}{\beta r} \overset{5}{e^{-\beta r}} G_2(()). \tag{19}$$

Where, "$y_{-2}(ar) = a\sinh(ar) - \frac{1}{r}\cosh(ar), y_2(ar) = a\cosh(ar) - \frac{1}{r}\sinh(ar)$" and $G_2(()$ is Gegenbauer function expounded in Abramowitz and Stegun[42]. The couple stress parameter $\beta = r_\circ \sqrt{\frac{\frac{r}{\mu}}{\eta}} = r_\circ \beta$, where the length-dependent parameter $\sqrt{\frac{\eta}{\mu}}$ is a characteristic measure of the polarity of the couple stress fluid models.

3 | BOUNDARY CONDITIONS

For this particular problem, the following boundary constraints are both physically realistic and systematically consistent.

On the surface of a solid spherical core $R = a_o$ **:** No slip boundary conditions are imposed

$$\mathbf{q_r}^{(2)} = 0 \quad (i.e.)\ \ \psi_\Theta^{(2)} = 0. \tag{20}$$

$$\mathbf{q_\theta}^{(2)} = 0 \quad (i.e.) \quad \psi_r^{(2)} = 0. \tag{21}$$

On the fluid porous interface $R = a$**:** We assume the continuity of tangential velocity, tangential stress and vanishing couple stress as,

$$\mathbf{q_\theta}^{(1)} = \mathbf{q_\theta}^{(2)} \quad (i.e.)\ \ \psi_r^{(1)} = \psi_r^{(2)}. \tag{22}$$

$$r_{r\Theta}^{(1)} = r_{r\Theta}^{(2)}. \tag{23}$$

$$m_{rø} = 0. \tag{24}$$

On the outer cell surface at $R = b$ **(i.e.)** $r = l\ (\ ^{-1}) = b/a$**:** The boundary constraints on the cell surface at $R = b$ are reduced from a complex to a simple problem. All four models, as well as the radial velocity of the liquid sphere on the cell surface, are taken into consideration, $\mathbf{q}_r\ ^{(1)} = U\cos\Theta$ that is,

$$\frac{6\psi^{(1)}}{6\Theta} = r^2 \sin\Theta\cos\Theta. \tag{25}$$

(i) Happel Model[12]: The Happel model suggests the absence of tangential viscous stresses on the cell surface ($r = b$), $r_{r\theta}^{(1)} = 0$ that is,

$$2r\frac{\partial}{\partial r}\left[\frac{1}{r}\frac{\partial\psi^{(1)}}{\partial r}\right] - \frac{\partial^2\psi^{(1)}}{\partial r^2} + \frac{1}{r^2}\frac{\partial^2\psi^{(1)}}{\partial\theta^2} - \frac{\cot\theta}{r^2}\frac{\partial\psi^{(1)}}{\partial\theta} = 0. \tag{26}$$

(ii) Kuwabara Model[14] : The absence of vorticity (flow potentiality) on the cell surface is imposed as follows by the Kuwabara model $\mathrm{A} \times \mathbf{q} = 0$ that is,

$$\frac{\partial^2\psi^{(1)}}{\partial r^2} + \frac{1}{r^2}\frac{\partial^2\psi^{(1)}}{\partial\theta^2} - \frac{\cot\theta}{r^2}\frac{\partial\psi^{(1)}}{\partial\theta} = 0. \tag{27}$$

(iii) Kvashnin Model[15]: Kvashnin model assumes, the cell symmetry condition, $\frac{\partial q_\theta^{(1)}}{\partial r} = 0$ that is,

$$\frac{1}{r}\frac{\partial\psi^{(1)}}{\partial r} - \frac{\partial^2\psi^{(1)}}{\partial r^2} = 0. \tag{28}$$

(iv) Mehta - Morse Model[16]: The homogeneity on the cell surface $q_\theta^{(1)} = -\sin\theta$ that is

$$\frac{\partial\psi^{(1)}}{\partial r} = r\sin^2\theta. \tag{29}$$

Solving all boundary conditions from the equations (20) to (29) using (18) and (19), we get the algebraic linear equations to different models. Using the MATHEMATICA software, we can find the unknown constants A_1, B_1, C_1, D_1, A_2, B_2 and C_2 by making use of the equations (18) and (19) into the boundary constraints (20) – (25), and one boundary constraint from (26) - (29) yields in a set of equations to different four models.

4 | EVALUATION OF THE HYDRODYNAMIC DRAG FORCE AND HYDRODYNAMIC PERMEABILITY

The most important feature of the problem is the hydrodynamic drag force $\tilde{F}$ acting on a spherical droplet with a uniformly structured permeable spherical container and can be calculated using the simple formula

$$\tilde{F} = 4\pi\mu_1 a^2 U a \lim_{r\to\infty}\left[\frac{\psi^{(1)} - \psi_\infty^{(1)}}{c^2}\right]. \tag{30}$$

where, $c = r\sin\theta$, ψ_∞ is the stream function of the fluid motion at infinity. In this present situation, the modified expression is

$$\tilde{F} = 2\pi\mu_1 a U a^2 B_1. \tag{31}$$

The hydrodynamic drag coefficient can be defined as follows,

$$D_N = \frac{\tilde{F}}{-2\pi\mu_1 U a}. \tag{32}$$

The hydrodynamic permeability L_{11} is defined as the rate of uniform flow ratio U to the pressure of cell gradient $\tilde{F}/\tilde{V}$ [43]. Thus

$$L_{11} = \frac{U}{\tilde{F}/\tilde{V}}. \tag{33}$$

Where, $\tilde{V} = \frac{4}{3}\pi\tilde{c}^3$ ($\tilde{V}$ - volume of the spherical container). The hydrodynamic permeability L_{11} of the homogeneous porous spherical container can be calculated by making use of the values of the drag force F from equation (31) and the volume of the spherical container $\tilde{V}$. Thus,

$$L_{11} = -\frac{1}{3\mu_1}\frac{\tilde{c}^3}{B_1} = L_{11}\frac{\tilde{b}^3}{\mu_1}. \tag{34}$$

Where, $\gamma^3 = \frac{\tilde{c}^3}{\tilde{a}^3}$ and $L_{11} = -1/3\gamma^3 B_1$ is the dimensionless hydrodynamic permeability.

5 | SPECIAL CASES

Case (i): If $l \to \infty$ and $a \to 0$, a couple stress fluid sphere emerges from a porous sphere in an unbounded expanse. As an outcome, the drag force value is

$$F^{\sim} = -6\,a\,л\,U\mu_1 \quad 1 + \frac{s}{\beta} \quad . \tag{35}$$

Where, $s = \frac{2+r}{2+r+\beta}$, $r = \frac{\eta^f}{\eta}$, $\beta = \frac{r}{l}$. This is the well-familiar result formerly achieved by Ramkissoon[44].

Case (ii): If the couple stress viscosity vanishes ($\eta \to 0$) that is $\beta \to \infty$ then the non-Newtonian couple stress fluid sphere behaves like a Newtonian viscous fluid sphere. As a result, the drag force $F^{\sim}$ on a Newtonian fluid medium as follows,

$$F^{\sim} = -6\,a\,л\,U\mu_1 \quad \frac{0_{4/3ð} - 1^{1}}{2ð - 1} \quad , \qquad ð = \frac{\mu_1}{\mu_2}. \tag{36}$$

This result coincides with the earlier result for the drag, which is given by the Happel and Brenner[43] book.

Case (iii): If $\beta \to 0$ and $r \to 0$ the drag on the porous sphere with radius ${}^{f}a^{f}$ in a cell with radius ${}^{f}b^{f}$ is given by,

For Happel model:

$$F = 2aлU(a(a^4 + a^2(3 - 9\ {}^{1/3} + 6\ {}^{2/3}) - 18(-\ {}^{2/3} + \ ))(+ 3(a^4(-1+ \\ {}^{1/3}) + 6\ + a^2(3\ {}^{1/3} - 6\ {}^{2/3} + 2\ ))3)\mu_1/a(a^2(-1 + \ ) - 6\ {}^{2/3} \\ + 3\ - 9\ {}^{4/3})(+ 3(4a\ + \ {}^{1/3}(-2\ {}^{2/3} + 3\ + a^2(-1 - \ {}^{2/3} + \ ))3). \tag{37}$$

For Kuwabara model:

$$\tilde{F} = 2aлUa^2(6a\ {}^{1/3}(+ 6a^2 3 - 2(3 + a^2)3 - 2a(3 + a^2)()\mu\ / \\ 3a\ {}^{\frac{4}{3}}(+ \ {}^{\frac{1}{3}}(-a^{2}(-1 + \ ) - 3\ )3 + 3a^{2}3 + (-a^{3}(-1 + \ ) - 3\ )(. \tag{38}$$

For Kvashnin model:

$$F = 2aлU(a(a^4 + 3a^2(-1 + \ {}^{1/3})^2 + 9\ {}^{2/3} - 9\ )(+ (a^4(-3 + 2\ {}^{1/3}) \\ + 9\ + 3a^2(2\ {}^{1/3} - 3\ {}^{2/3} + \ ))3)\mu_1/6a\ + a(a^2(-1 + \ ) - 3(\ {}^{2/3} - \\ + 2\ {}^{4/3}))(+ \ {}^{1/3}(-3\ {}^{2/3} + 6\ + a^2(-2 - 3\ {}^{2/3} + 2\ ))3. \tag{39}$$

For Mehta-Morse model:

$$F = 2aлU(3a(a^2 - 3\ {}^{1/3})(-1 + \ {}^{1/3})(+ (a^4 + 3a^2(1 - 3\ {}^{1/3}+ \\ {}^{2/3}) + 9\ {}^{2/3})3)\mu_1/6a\ {}^{2/3} - 3a(\ {}^{1/3} + \ )(+ (a^2(-1 + \ )+ \\ 3(-\ {}^{2/3} + \ ))3. \tag{40}$$

where, $\cosh[a - \frac{a}{1/3}] = (, \sinh[a - \frac{a}{1/3}] = 3$. These are the most recent results for a couple stress fluid spheres embedded in porous medium.

Case (iv): If, $a \to 0, \beta \to 0$ and $r \to 0$ then the drag force turns out as,
For Happel model:

$$\tilde{F} = \frac{4aлU(3 + 2\ {}^{5/3})\mu_1}{-2 + 3\ {}^{1/3} - 3\ {}^{5/3} + 2\ {}^{2}}. \tag{41}$$

This well-known outcome is the same as that previously reported by Happel[12].

For Kuwabara model:

$$\tilde{F} = \frac{30aлU\mu_1}{-5 + 9\ {}^{1/3} - 5\ + \ {}^{2}}. \tag{42}$$

This was an earlier result of Kuwabara[14].

For Kvashnin model:

$$\tilde{F} = \frac{24a\pi U(4 + \ ^{5/3})\mu_1}{-16 + 27\ ^{1/3} - 10\ \ -9\ ^{5/3} + 8\ ^{2}}. \tag{43}$$

This finding is consistent with what Kvashnin previously reported[15].

For Mehta-Morse model:

$$\tilde{F} = \frac{24a\pi U(-1 + \ ^{5/3})\mu\ \ _1}{(-1 + \ ^{1/3})\ ^4(4 + 7\ ^{1/3} + 4\ ^{2/3})}. \tag{44}$$

The well-known outcome is consistent with Mehta-Morse's earlier findings[16].

Case (v): When $\rightarrow 0$, the drag on a solid sphere in an infinite expanse is given by

$$\tilde{F} = -6a\pi U\mu_1. \tag{45}$$

Stokes[45] previously reported a similar result.

6 | RESULTS AND DISCUSSION

At low Reynolds numbers, the non-dimensional drag coefficient D_N acting on the porous medium using an in cell-model is discussed. The various parameters are as follows:

- The volume fraction of the particle $(0 < \ < 1)$.
- The permeability parameter a.
- The classical viscosity ratio between internal and surrounding fluids δ.
- Couple stress parameter β.
- Couple stress viscosities η and η^f.

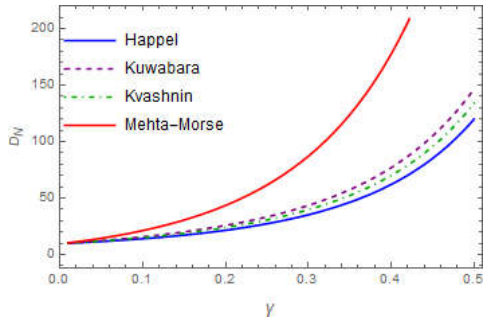

FIGURE 2 Variation of drag coefficient with volume fraction

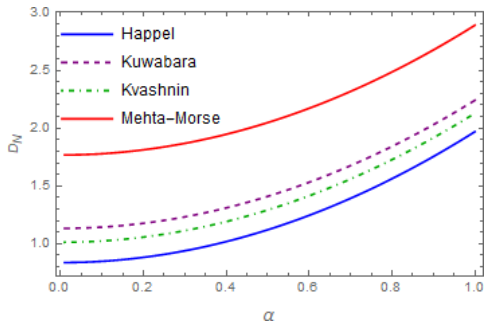

FIGURE 3 Variation of drag coefficient with permeability

The figures show the hydrodynamic drag force and hydrodynamic permeability results for a viscous fluid sphere in unit cell model. The dependences of the drag coefficient D_N for suspension of a motion of couple stress fluid sphere ($\delta = 0,\ \delta = 1,\ \delta \rightarrow \infty$) given by equation (32) for all four (Happel, Kuwabara, Kvashnin, Mehta-Morse) cell models individually, monotonically increases with an increase in for any predetermined finite values of penetrability parameter a, couple stress parameter β for all four models concur for low fraction of volume. The drag with $\delta = 0$ addresses the outcome for the rigid sphere in cell, and the drag with $\delta \rightarrow \infty$ addresses the outcome for the spherical bubbles. It is noticed that the drag D_N grows up with increasing volume fraction. It is interesting to observe that for the beginning stage the growth of D_N is almost

equal for all four models. Besides, the proposed model presents a mathematical examination in Table 1 (Appendix).

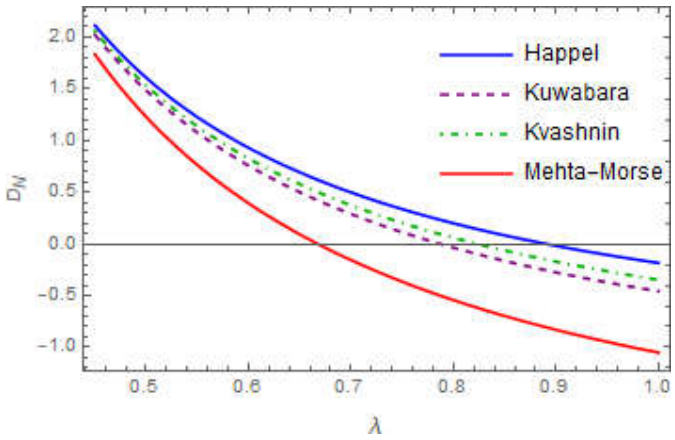

FIGURE 4 Variation of drag coefficient with couple stress parameter

From the figure 2 it is discovered that a rigid sphere-in-cell has a higher drag and spherical bubbles have a lower drag coefficient. While adjoining fluid particles are adequately near each other, an enormous pressure gradient creates between them, causing more drag coefficient, though when is a small, adjoining molecule significantly affect the flow around a fluid sphere. When contrasted with different models, is somewhat higher for the Mehta-Morse model. Variations in dimensionless drag coefficient D_N with permeability for each of the four models are displayed in figure 3 . It very well may be seen that as the permeability parameter increases (the specific permeability of the porous medium decreases), the drag coefficient rapidly increases. In case of concentrated media, the Mehta-Morse model shows a deviation in permeability from the four models. This reality can be explained mathematically in the accompanying manner. The Happel, Kuwabara, Kvashnin boundary conditions all utilization similar terms in various combinations, while the Mehta-Morse condition contrasts altogether from the others. According to an actual viewpoint, the Mehta-Morse condition, which is getting together with the uniform flow at the cell boundary, is the most troublesome of the four kinds of limit conditions considered. This condition should bring about increased energy scattering in a system.

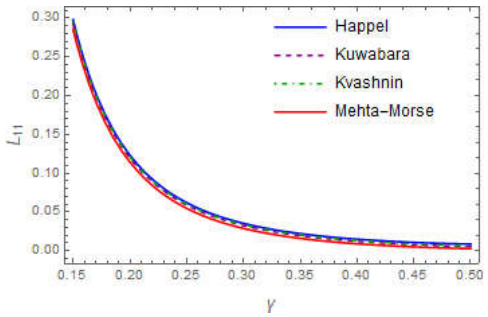

FIGURE 5 Variation of hydrodynamic permeability with volume fraction

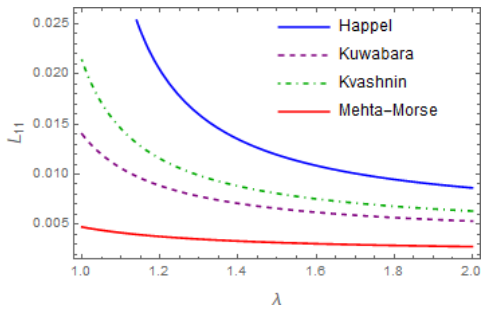

FIGURE 6 Variation of hydrodynamic permeability with couple stress parameter

Figure 4 depicts how the drag increases as the couple stress parameter is increased when the fixed values of δ and r. It very well may be seen that the drag force at first abatements quickly then, at that point, step by step diminishes and ultimately turns out to be consistent. The fundamental justification behind this minor drag impact is that the parameter of couple stress viscosity η is likewise present in the dimensionless couple stress parameter β. The Mehta-Morse model deviates from the other three

models when applied to concentrated media. The following mathematical method can be used to explain this reality. While the Mehta-Morse condition differs significantly from the others, the Happel, Kuwabara, and Kvashnin boundary conditions all use similar terms in different combinations. The Mehta-Morse condition, which interacts with uniform flow at the cell boundary, is actually the most challenging of the four types of limit conditions taken into consideration. This circumstance ought to increase the system's energy scattering.

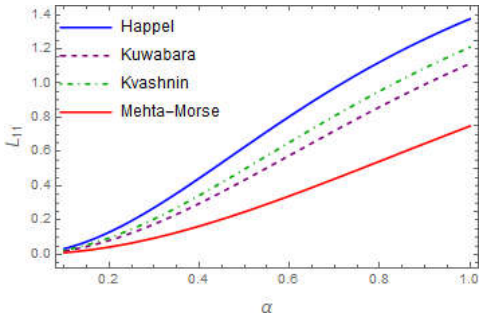

FIGURE 7 Variation of hydrodynamic permeability with permeability parameter

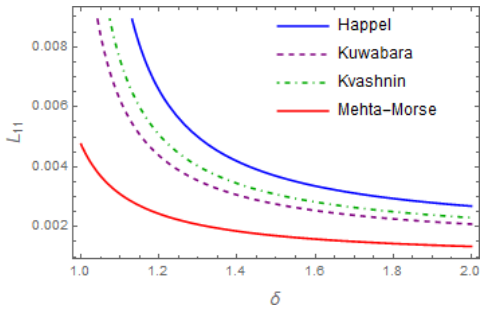

FIGURE 8 Variation of hydrodynamic permeability with viscosity ratio

The impact of the volume fraction on the hydrodynamic drag force applied on the spherical droplet is portrayed in figure 5 . It is noticed that the growth rate of hydrodynamic permeability decreases with the increasing medium volume fraction, and as → 1, the variation is almost steady. Figure 6 depicts how the hydrodynamic permeability increases as the couple stress parameter is increased. It can be seen that the hydrodynamic permeability initially decreases rapidly when ($1.0 \leq \beta \leq 1.2$), then gradually decreases and eventually becomes steady. It is worth mentioning that as the couple stress viscosity ratio increases, so does the hydrodynamic permeability. The variety of the hydrodynamic porousness and dimensionless penetrability boundary is displayed in figure 7 . It is seen that the development rate of hydrodynamic permeability increases with the increasing medium penetrability. Further, the pace of rot increments when contrasted with different models is somewhat higher for the Happel cell model. Figure 8 deciphered that the reliance of the non-dimensional hydrodynamic penetrability on viscosity ratio. From this figure, we presume that the hydrodynamic penetrability diminishes as viscosity ratio.

7 | CONCLUSION

The purpose of this study is to explore the cell model for uniform fluid flow through a couple stress fluid covered by a porous medium. The Brinkman and Stokes equations govern the flow through the porous spherical container and the couple stress fluid spherical droplet respectively. The components of the velocity profile are calculated by using stream functions, and the sphere's surface is subjected to kinematic viscosity of mutual impenetrability, the continuity of tangential velocity and tangential stresses, vanishing couple stresses, Happel, Kuwabara, Kvashnin, and Mehta-Morse (Cunningham's) boundary constraints. For the axially symmetric motion, both pressure distribution and the stream function solution are explicitly solved. The method of variable separation is used to investigate an analytical resoluteness for the flow field. The drag force on an Uniform fluid flow through a non-Newtonian couple stress fluid covered by a porous medium in cell model and the drag coefficient are calculated, and the impacts of the permeability, the ratio of viscosity, the couple stress viscosity ratio, and the parameter of couple stress . The appropriate dependencies are graphically delineated and reviewed, including the permeability, couple stress parameter, viscosity ratio, and couple stress viscosities. The consequences of a wide range of appropriate parameters on hydrodynamic drag force and hydrodynamic permeability have been examined and graphically presented. The following are some of the major findings:

1. The growth of the drag coefficient is almost equal for all four models. Nonetheless, for somewhat high values of particle volume, a significant increase is noticed for each of the four models. It has been discovered that a rigid sphere-in-cell has a higher drag and spherical bubbles have a lower drag.

2. The variation of the drag coefficient with the couple stress parameter in the Happel, Kuwabara, Kvashnin, Mehta-Morse models is observed. It is clear that as the couple stress viscosity proportion increases, so does the drag. The main reason for this minor drag effect is that the couple stress viscosity parameter is likewise present in the non-dimensional couple stress parameter.
3. Variations in dimensionless coefficient with permeability parameter for all four models are noticed. It can be seen that as the permeability parameter increases (the specific permeability of the porous medium decreases), the drag coefficient rapidly increases.
4. It is observed that the growth rate of hydrodynamic permeability diminishes with the increasing medium volume fraction.
5. Hydrodynamic permeability increases as the parameter of couple stress is increased.
6. The growth rate of hydrodynamic permeability increases with the increasing medium permeability.
7. The hydrodynamic permeability decreases as viscosity ratio.

Future work may investigate the couple stress fluid saturated with a porous medium in different geometric shapes with no-slip and slip boundary conditions in a permeable medium. A few applications of the current problem include determining the drag of droplets through an obstacle, segregation of minerals such as uranium and gold, extraction of proteins and other macromolecules in pharmaceutical and biological processes, and municipal garbage treatment, among others.

ACKNOWLEDGMENTS

The referee(s) are appreciated by the authors for their correction suggestions, which significantly enhanced the manuscript. The Excel Engineering College (Autonomous) in Namakkal is also acknowledged by the authors for helping to support this work.

References

[1] D Josef, L Tao, *Zamm* **1964**, *44*, 361.

[2] Vijay Kumar Stokes in *Theories of fluids with microstructure*, Springer, **1984**, pp. 34–80.

[3] Vijay Kumar Stokes, *The Physics of Fluids* **1968** *11*(5), 1131.

[4] Vijay Kumar Stokes in *Theories of fluids with microstructure*, Springer, **1984**, pp. 150–178.

[5] S L Rao, T K V Iyengar, *UGC Research project C-8-4/82 SR III* **1985**.

[6] H Ramkissoon, *Zeitschrift für angewandte Mathematik und Physik ZAMP* **1978** *29*(2), 341.

[7] M Devakar, T K V Iyengar, *Nonlinear Analysis: Modelling and Control* **2008** *13*(2), 181.

[8] B S Padmavathi, T Amaranath, *Zeitschrift für angewandte Mathematik und Physik ZAMP* **1993** *44*(1), 178.

[9] Qin Yu, P N Kaloni, *Journal of engineering mathematics* **1988** *22*(2), 177.

[10] T Zlatanovski, *The Quarterly Journal of Mechanics and Applied Mathematics* **1999** *52*(1), 111.

[11] J V Ramana Murthy, N Srinivasacharyulu, P Aparna, *Bull. Cal. Math. Soc* **2007** *99*(3), 293.

[12] John Happel, *AIChE journal* **1958** *4*(2), 197.

[13] John Happel, *AIChE Journal* **1959** *5*(2), 174.

[14] Sinzi Kuwabara, *Journal of the physical society of Japan* **1959** *14*(4), 527.

[15] AG0422 Kvashnin, *Fluid Dynamics* **1979** *14*(4), 598.

[16] Gurmukh Dass Mehta, T F Morse, *The Journal of Chemical Physics* **1975** *63*(5), 1878.

[17] EI29937751293 Saad, *Meccanica* **2012** *47*(8), 2055.

[18] E I Saad, *Meccanica* **2013** *48*(7), 1747.

[19] P Aparna, P Padmaja, N Pothanna, J V Ramana Murthy, *Nonlinear Engineering* **2020** *9*(1), 352.

[20] P Aparna, N Pothanna, J V R Murthy in *Advances in Fluid Dynamics*, Springer, **2021**, pp. 135–146.

[21] M Devakar, B Shankar, *Solid State Technology* **2021** *64*(2), 1418.

[22] M Devakar, K Ramesh, K Vajravelu, *Journal of Computational Mathematics and Data Science* **2022**, *2*, 100025.

[23] Tarek Shehadeh, Emad Ashmawy, *BAU Journal-Science and Technology* **2019** *1*(1), 8.

[24] Noura S Alsudais, Shreen El-Sapa, E A Ashmawy, *European Journal of Mechanics-B/Fluids* **2022**, *91*, 244.

[25] T S L Radhika, T Raja Rani, Divy Dwivedi **2020**.

[26] T S L Radhika, Others, *MATEMATIKA: Malaysian Journal of Industrial and Applied Mathematics* **2021**, 15.

[27] D Srinivasacharya, I Sreenath, *International Journal of Applied and Computational Mathematics* **2020** *6*(2), 1.

[28] K M Surabhi, Arpitha Ravikanti, D Srikanth, D Srinivasacharya, *Applied Mathematics-A Journal of Chinese Universities* **2021** *36*(4), 492.

[29] A N Filippov, Yu O Koroleva, A K Verma, *Membranes and Membrane Technologies* **2020** *2*(4), 230.

[30] Ramasamy Selvi, Pankaj Shukla, A N Filippov, *Colloid Journal* **2020** *82*(2), 152.

[31] R Selvi, Pankaj Shukla, Abhishek Kumar Singh, *Journal of Porous Media* **2020** *23*(6).

[32] D Yu Khanukaeva, A N Filippov, P K Yadav, A Tiwari, *European Journal of Mechanics-B/Fluids* **2019**, *76*, 73.

[33] Ramalakshmi Krishnan, Pankaj Shukla, *ZAMM-Journal of Applied Mathematics and Mechanics/Zeitschrift für Angewandte Mathematik und Mechanik* **2021** *101*(11), e202000115.

[34] V Geetha Vani, A S V Ravi Kanth, in *AIP Conference Proceedings*, AIP Publishing LLC, **2020**, p. 30020.

[35] Sakthivel Shyamala, Pankaj Shukla, *Journal of Porous Media* **2022** *25*(8).

[36] Shyamala Sakthivel, Pankaj Shukla, *Special Topics & Reviews in Porous Media: An International Journal* **2023** *14*(1).

[37] Shyamala Sakthivel, Pankaj Shukla, *ZAMM-Journal of Applied Mathematics and Mechanics/Zeitschrift für Angewandte Mathematik und Mechanik* **2023**, e202200601.

[38] Sakthivel Shyamala, Pankaj Shukla, Ramasamy Selvi, *Journal of Porous Media* **2024** *27*(7), 85.

[39] Sara I Abdelsalam, Abdullah Madhi Alsharif, Y Abd Elmaboud, AI Abdellateef, *Heliyon* **2023** *9*(5).

[40] Sara I Abdelsalam, A Magesh, P Tamizharasi, AZ Zaher, *International Journal of Numerical Methods for Heat & Fluid Flow* **2023**.

[41] Sara I Abdelsalam, MM Bhatti, *Scientific Reports* **2023** *13*(1), 5684.

[42] M Abramowitz, I A Stegun.

[43] John Happel, Howard Brenner in *Low Reynolds number hydrodynamics*, Springer, **1983**, pp. 431–473.

[44] H Ramkissoon, *Zeitschrift für angewandte Mathematik und Mechanik* **1998**, *78*.

[45] George Gabriel Stokes, Others **1851**.

[46] Shyamala Sakthivel, Pankaj Shukla, Selvi Ramasamy, *Journal of Porous Media* **2024**, *27*.

APPENDIX

TABLE 1 Hydrodynamic permeability of the spherical container in unit cell for the various values of the volume fraction and couple stress viscosity with $\beta = 1$, $\delta = 1$.

	$\delta = 1$	$\delta = 0$	$\beta = 10$	$\beta = 20$	$\beta = 50$	$\beta = 100$	$\beta \to \infty$
Happel Model							
0.01	264.0889	2468.1063	830.9000	821.4706	818.46808	818.00259	817.84152
0.02	32.85681	308.35986	103.70843	102.52974	102.15443	102.09624	102.07610
0.03	9.64863	91.27995	30.64190	30.29265	30.18145	30.16421	30.15824
0.04	4.02307	38.46181	12.87973	12.73239	12.68547	12.67820	12.67568
0.05	2.03243	19.66543	6.56712	6.49168	6.46766	6.46393	6.46265
0.06	1.15930	11.36387	3.78359	3.73993	3.72603	3.72387	3.72312
0.07	0.71902	7.14546	2.37167	2.34417	2.33542	2.33406	2.33359
0.08	0.47412	4.77957	1.58129	1.56287	1.55700	1.55610	1.55578
0.09	0.32759	3.35168	1.10521	1.09227	1.08815	1.08752	1.08729
0.10	0.23483	2.43964	0.80174	0.79230	0.78930	0.78883	0.78867
0.20	0.02426	0.30190	0.09521	0.09403	0.09365	0.09359	0.09357
Kuwabara Model							
0.01	264.0090	2468.0263	830.82011	821.39066	818.38816	817.92267	817.76160
0.02	32.76302	308.26447	103.61422	102.43554	102.06023	102.00204	101.98191
0.03	9.58564	91.21421	30.57820	30.22897	30.11777	30.10053	30.09456
0.04	3.98155	38.41689	12.83735	12.69002	12.64311	12.63584	12.63332
0.05	2.00380	19.63300	6.53753	6.46211	6.43809	6.43437	6.43308
0.06	1.13861	11.33912	3.76189	3.71825	3.70435	3.70220	3.70145
0.07	0.70348	7.12568	2.35509	2.32761	2.31886	2.31751	2.31704
0.08	0.46208	4.76312	1.56818	1.54978	1.54392	1.54301	1.54270
0.09	0.31801	3.33755	1.09455	1.08163	1.07752	1.07688	1.07666
0.10	0.22706	2.42717	0.79286	0.78345	0.78045	0.77999	0.77983
0.20	0.02246	0.29372	0.09222	0.09106	0.09069	0.09063	0.09061
Kvashnin Model							
0.01	264.0430	2468.0603	830.85410	821.42465	818.42215	817.95666	817.79559
0.02	32.80018	308.30226	103.65154	102.47286	102.09755	102.03936	102.01923
0.03	9.60994	91.23958	30.60278	30.25354	30.14234	30.12510	30.11913
0.04	3.99739	38.43402	12.85351	12.70618	12.65927	12.65200	12.64948
0.05	2.01466	19.64530	6.54875	6.47332	6.44930	6.44558	6.44429
0.06	1.14643	11.34847	3.77009	3.72644	3.71255	3.71039	3.70965
0.07	0.70934	7.13314	2.36134	2.33386	2.32511	2.32375	2.32328
0.08	0.46661	4.76931	1.57312	1.55471	1.54885	1.54794	1.54763
0.09	0.32162	3.34289	1.09856	1.08564	1.08152	1.08088	1.08066
0.10	0.22998	2.43186	0.79620	0.78678	0.78378	0.78331	0.78315
0.20	0.02313	0.29677	0.09334	0.09217	0.09180	0.09174	0.09172
Mehta-Morse Model							
0.01	263.7816	2467.7984	830.59259	821.16314	818.16064	817.69515	817.53409
0.02	32.58403	308.08243	103.43445	102.25578	101.88047	101.82229	101.80216
0.03	9.47916	91.10309	30.47054	30.12133	30.01014	29.99290	29.98693
0.04	3.91474	38.34460	12.76915	12.62185	12.57495	12.56767	12.56516
0.05	1.95883	19.58208	6.49107	6.41567	6.39166	6.38794	6.38665
0.06	1.10656	11.30080	3.72829	3.68467	3.67078	3.66863	3.66788
0.07	0.67961	7.09529	2.32962	2.30217	2.29343	2.29207	2.29161
0.08	0.44368	4.73799	1.54815	1.52978	1.52393	1.52302	1.52271
0.09	0.30344	3.31605	1.07833	1.06544	1.06133	1.06070	1.06048
0.10	0.21526	2.40826	0.77940	0.77001	0.76703	0.76656	0.76640
0.20	0.01975	0.28166	0.08773	0.08660	0.08625	0.08619	0.08617